


RESEARCH ARTICLE | APRIL 03 2025

Ionization effects in single-shot carrier-envelope phase detection with gas-gap devices

Johannes Blöchl ; Maximilian F. Seeger; Hartmut Schröder ; Minjie Zhan ; Alexander Guggenmos ; Thomas Nubbemeyer ; Matthias F. Kling ; Boris Bergues  

 Check for updates

Appl. Phys. Lett. 126, 131106 (2025)

<https://doi.org/10.1063/5.0246794>

 CHORUS



Articles You May Be Interested In

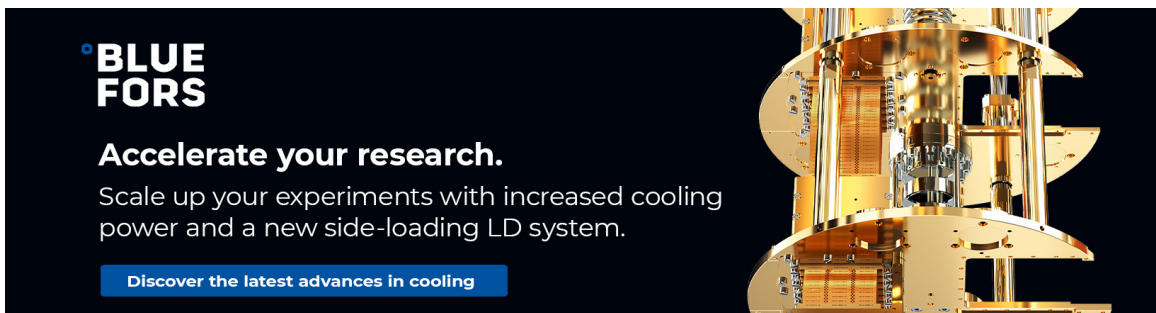
Space–time characterization of ultrashort laser pulses: A perspective

APL Photonics (July 2024)

Examination of optimized ultrashort three-color waveforms for generating short and intense isolated attosecond pulses in soft x rays

Appl. Phys. Lett. (July 2024)

30 April 2025 09:00:18



BLUE FORS

Accelerate your research.
Scale up your experiments with increased cooling power and a new side-loading LD system.

[Discover the latest advances in cooling](#)

Ionization effects in single-shot carrier-envelope phase detection with gas-gap devices

Cite as: Appl. Phys. Lett. **126**, 131106 (2025); doi: [10.1063/5.0246794](https://doi.org/10.1063/5.0246794)

Submitted: 2 December 2024 · Accepted: 13 March 2025 ·

Published Online: 3 April 2025



View Online



Export Citation



CrossMark

Johannes Blöchl,^{1,2,3} Maximilian F. Seeger,^{1,2} Hartmut Schröder,² Minjie Zhan,³ Alexander Guggenmos,³ Thomas Nubbemeyer,^{1,2} Matthias F. Kling,^{1,2,4,5} and Boris Bergues^{1,2,3,a)}

AFFILIATIONS

¹Ludwig-Maximilians-University Munich, Department of Physics, Am Coulombwall 1, 85748 Garching, Germany

²Max Planck Institute of Quantum Optics, Hans-Kopfermann-Str. 1, 85748 Garching, Germany

³UltraFast Innovations GmbH, Dieselstr. 5, 85748 Garching, Germany

⁴SLAC National Accelerator Laboratory, 2575 Sand Hill Rd., Menlo Park, California 94025, USA

⁵Applied Physics Department, Stanford University, 348 Via Pueblo, Stanford, California 94305, USA

^{a)} Author to whom correspondence should be addressed: boris.bergues@mpq.mpg.de

ABSTRACT

The carrier-envelope phase (CEP) is a key parameter for attosecond waveform control of ultrashort laser pulses. For laser systems with high repetition rates, however, single-shot CEP detection is still challenging. Building on recent findings on phase detection with electric current generation in gases, we show that with an optimized detection method, a long-term stable single-shot phase detection is feasible. We investigate the achievable performance depending on various parameters such as pulse duration, gas pressure, or incident intensity. The latter exhibits a regime where the saturation of the ionization process boosts the phase sensitivity of the signal, which is elucidated by numerical calculations.

© 2025 Author(s). All article content, except where otherwise noted, is licensed under a Creative Commons Attribution (CC BY) license (<https://creativecommons.org/licenses/by/4.0/>). <https://doi.org/10.1063/5.0246794>

Carrier-envelope phase (CEP) detection plays a central role in ultrafast science.^{1–3} Its detection in a single-shot manner has been demonstrated using the stereo above-threshold-ionization (ATI) phasemeter technique,⁴ which relies on the CEP dependence of characteristic spectral features of strong field photoionization spectra.⁵ Single-shot CEP detection based on spectral interference has also been demonstrated⁶ with achievable performances comparable to that of the stereo ATI phasemeter.⁷ Several improved and fast detection schemes have been introduced recently.^{8,9} Besides these two major branches of CEP detection, other phenomena like currents in micro- or nanostructures,^{10–14} or the detection of laser-induced currents in solids^{15,16} and gases,^{17–19} have emerged as CEP sensing techniques in recent years. Except Refs. 10, 12, 14–16, 18, all of them have been demonstrated in single-shot mode.

Here, we adopt the principle presented in Ref. 17, which is based on the detection of spatially directed currents from strong field ionization of ambient air driven by circularly polarized laser pulses. In contrast to Refs. 17 and 20, the present setup uses linearly polarized laser pulses and is therefore applicable to most few-cycle laser systems. Long-term stability of single-shot CEP measurements has been demonstrated with

the stereo ATI phasemeter^{21,22} and the f-2f interferometer.⁷ With our setup, we show that long-term stability (of several hours) of single-shot CEP detection is also achievable with a gas-gap device.

The signal formation and the CEP sensitivity has been studied in gas-gap^{18,23} or nanoplasmonic^{10,13,14,24–26} devices. Especially for the latter, the incident intensities could be kept low owing to the field enhancement. Here, in contrast, the intensity is high enough to drive the target ionization into saturation. Investigating how the achievable performance varies as a function of intensity and target gas pressure, we observe a boost of the CEP sensitivity in the saturation regime. This effect is explained by a theoretical model of the initial signal formation.

The experiments are conducted using a titanium-sapphire laser system (Femtolasers Femtopower HR 10 kHz, Rainbow oscillator with CEP4), equipped with a hollow-core fiber spectral broadening system and a chirped mirror compressor (UltraFast Innovations PC70). The pulse duration after compression is 4.5 fs, as determined via a d-scan measurement,²⁷ with a shot-to-shot intensity fluctuation of approximately 1%.

The experimental setup for the single-shot phase detection is outlined in Fig. 1(a). Two foci are generated by sending the linearly

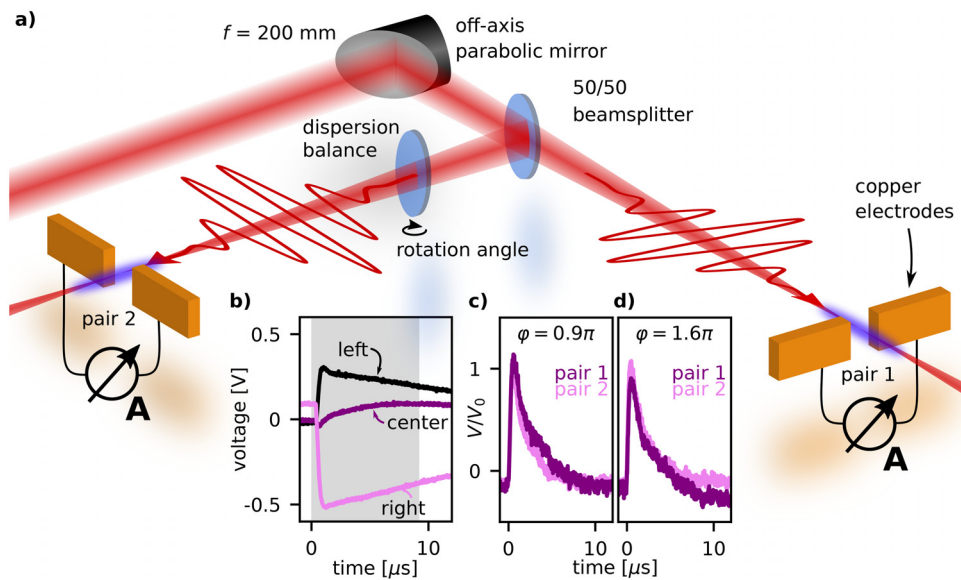


FIG. 1. (a) The laser beam is focused between two pairs of electrodes with a $f = 200$ mm parabolic mirror. (b) Signal of one electrode pair for different focus positions. The shaded area represents the time window over which the signal was integrated. (c) and (d) Phase dependence of the signal amplitude of both electrode pairs for a focus centered between them, normalized on the averaged value V_0 for random CEP.

p-polarized laser pulse onto a $f = 20$ cm off-axis parabolic mirror followed by a 50/50 UV-fused silica beam splitter. A glass plate in the reflected beam compensates the material dispersion of the beam splitter and adjusts the relative CEP in the two arms by its tilt. A pair of copper electrodes is placed in the vicinity of each focus. The distance between the electrodes is $350 \mu\text{m}$ —more than 10 times larger than the focal size of $25 \mu\text{m}$ full-width at half-maximum. Effects of the Gouy phase shift along the focus are minimized as the respective dimension of the copper electrodes of 0.5 mm is shorter than the Rayleigh length of 0.7 mm. Each electrode pair is encapsulated in a metal gas cell with optical windows (not shown in Fig. 1) allowing the pressure and gas type to be adjusted to maximal signal.¹⁸ To further increase the signal strength, the gas cell is filled with 3–10 mbar evaporated ethanol to exploit its lower ionization potential compared to air.

The laser-induced current between each pair of electrodes is transimpedance amplified (10^8 V/A, FEMTO DLPCA-200). The electrodes are not biased and therefore detect the laser-induced charge displacement rather than the total electron yield. The polarity of the detected signal mainly depends on the position of the focus relative to the electrodes [see Fig. 1(b)]. The signal amplitude crosses zero for a perfectly centered focus and becomes positive or negative when the focus is shifted toward one or the other electrode, respectively. We note that sometimes, a small electronic overshoot of the signal is present, as for the “center” measurement in Fig. 1. For a fixed focus position, the signal amplitude varies as a function of the CEP, as illustrated in Figs. 1(c) and 1(d). There, the signal of each electrode is plotted for different CEPs and divided by the CEP averaged signal amplitude. Subsequently, for single-shot detection, the resulting voltage signal is boxcar-integrated over a short time window [gray area in Fig. 1(b)] using homebuilt integrate-and-hold electronics. To maximize the signal-to-noise ratio, the CEP-independent contribution is minimized by centering the focus between the electrodes, which trims the offset and

enhances the contrast. The detected CEP is only a relative one as explained later.

Our detection scheme can be employed for single-shot CEP detection over extended acquisition times, reaching several hours, without realigning the experimental setup. The results of a more than 5 h measurement with randomized CEP are shown as a parametric plot (PP) in Fig. 2, where the signal of electrode pair 1 or 2 yields the x or y value, respectively. For that data, the phase shift between the electrodes is adjusted to $\approx 90^\circ$, as reflected by the circular shape of the PP. Following the re-centering procedure (Refs. 17 and 21), the running average of the electrode signal acquired over thousand consecutive shots is subtracted from the single-pulse signal. This procedure effectively removes the CEP-independent part of the signal. The data presented in Fig. 2 are recorded with an incident pulse energy of $30 \mu\text{J}$ at 6 mbar ethanol pressure and binned into 400 bins along both x and y axes before plotting in a polar coordinate system. The phase resolution $\Delta\varphi = \sigma_r/r$ is determined from the measured standard deviation σ_r of the radial width of the PP⁴ and amounts to 194 mrad considering all the data points in Fig. 2.

The rather large electrode distance of $350 \mu\text{m}$ enhances the long-term stability. Even though a larger gap size results in a signal reduction,¹⁸ we find that it reduces the sensitivity of the device to beam pointing fluctuations. In first order approximation, the sensitivity to pointing is the ratio of the pointing amplitude to the gap size.¹⁸ Thus, for a given beam pointing amplitude, a larger electrode distance results in smaller changes of the electric current.

For verification that the signal is proportional to the CEP of the laser pulse, we measure the CEP while varying it with the CEP shifter of the CEP-stabilized oscillator. The CEP retrieved from the data after re-centering^{17,21} and re-binning⁴ is compared to the nominal CEP for the applied voltage in Fig. 3(a). The agreement of both curves confirms that the retrieved CEP is directly proportional to the applied voltage.

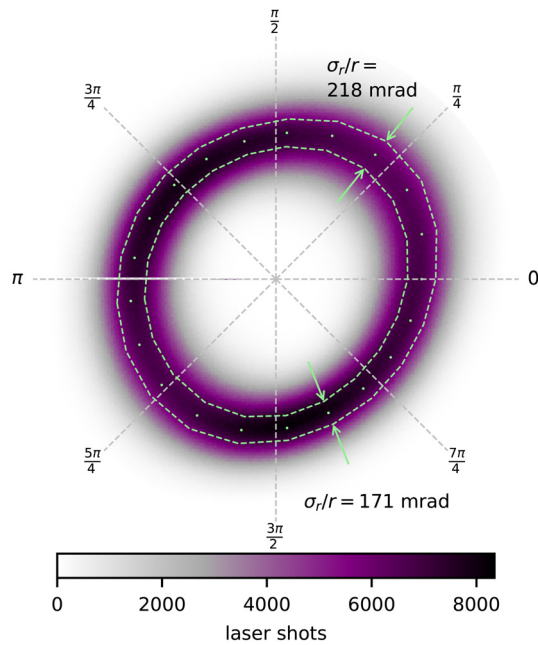


FIG. 2. Re-centered parametric plot obtained from an acquisition time of more than 5 h, corresponding to 1.8×10^6 consecutive laser pulses with random CEP. The dashed lines enclose a σ_r -interval around the mean radius.

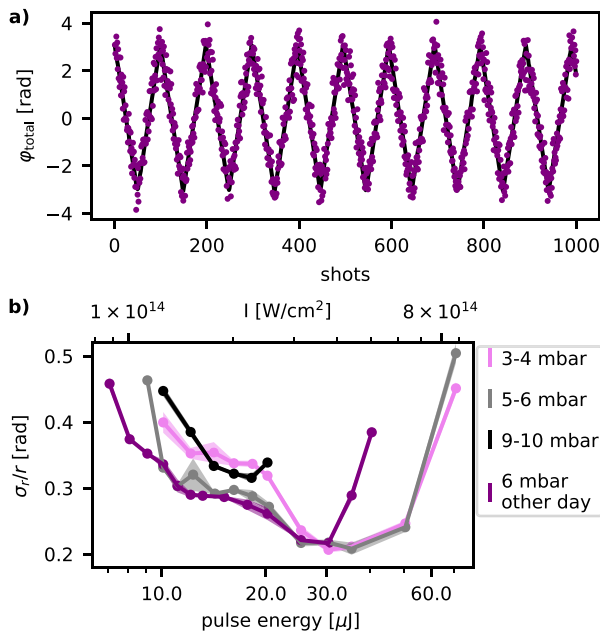


FIG. 3. (a) Comparison of the measured CEP (dots) to the nominal CEP (line). (b) Pressure and pulse energy scaling of the achievable precision of the device. The pulse energy is measured in front of the beam splitter, while the intensity represents the peak intensity in the focus.

The deviation of the data points in Fig. 3(a) from the nominal voltage, $\Delta\varphi_{\text{total}}$, consists of two contributions, the measurement error of the phasemeter, $\Delta\varphi$, and CEP fluctuations of the laser, $\Delta\varphi_{\text{laser}}$, faster than the CEP voltage scanning period. Since those noise sources are independent, we can write the total noise as $\Delta\varphi_{\text{total}} = \sqrt{\Delta\varphi^2 + \Delta\varphi_{\text{laser}}^2}$. With the device resolution of $\Delta\varphi \approx 226$ mrad [which is the width of the parametric plot corresponding to Fig. 3(a)], and the deviation of the CEP values from the nominal CEP of around 574 mrad, we can extract a CEP noise of the laser of 528 mrad. This is consistent with the shot-to-shot CEP stability of the laser of ≈ 600 mrad, which we determine with a fixed CEP voltage via the angular spread of the data in the PP and our CEP meter. This CEP noise of the laser does not transfer to an increased radial width of the PP as pure CEP drifts appear as angular spread of the data.

In Fig. 3(b), we scan the intensity for different pressures of the evaporated ethanol and observe an increase in CEP resolution at peak intensities around 4×10^{14} W/cm², where σ_r/r reaches its minimum. At higher intensities, the resolution decreases again. Best resolution is achieved at a pressure of a few millibars. For lower pressures, the signal amplitude decreases, leading to a collapse of the PP caused by the decreasing particle density and the correspondingly lower number of charge carriers. For a pressure of around 9 mbar, the measured data are only meaningful for intensities up to around 2×10^{14} W/cm². Above that intensity, the radial width of the PP increased significantly, preventing the CEP retrieval. The usage of ethanol yields a boost of the signal of nearly one order of magnitude as compared to air, which allows to reduce the incident intensity by about a factor of two.

Since saturation of the ionization process is expected to be significant at the intensities used in our experiment, it is crucial to incorporate this effect in the theoretical description. We model the strong field interaction between the few-cycle laser pulses and the ethanol molecules by solving the following rate equations:

$$N(t + dt) = N(t) - dN, \quad (1)$$

$$= N(t) - w(t + dt)dt \cdot N(t), \quad (2)$$

$$Z(t + dt) = Z(t) + dN. \quad (3)$$

Here, $N(t)$ is the ground state population of ethanol molecules, $N(t = t_0) = N_0$ is the initial population, $Z(t)$ is the total number of free electrons, and $w(t)$ is the ionization rate of ethanol. The latter is calculated using the statistical photoionization model (SPI) of Ref. 28. We prefer the SPI model over the commonly used Keldysh,²⁹ (molecular) ADK,^{30,31} or PPT³² ionization rates since it only relies on the single-photon absorption cross section and the ionization potential as an input, and can thus easily be applied to more complex molecules such as ethanol. The general applicability of the SPI model to a large range of atomic and molecular targets has been demonstrated in Ref. 28. Here, we calculate the ionization rate $w(t)$ using the single-photon absorption cross section of Ref. 33 and the ionization potential of 10.47 eV³⁴ for ethanol.

The electron emission rate $dZ(t)/dt$ is plotted in Fig. 4 (lower panel) for a 4.5 fs Gaussian pulse together with $w(t)$. At a representative peak field strength of 4.6×10^{10} V/m, the ionization process is driven into saturation, which is evidenced by the shift between $dZ(t)/dt$ and $w(t)$. This shift can be attributed to the depletion of the ground state before the peak of the electric field, which significantly reduces the electron yield in subsequent cycles due to the lower number of available neutral molecules. In an unsaturated scenario, in

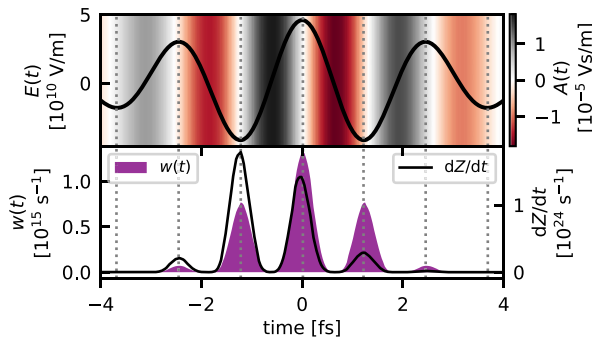


FIG. 4. Top: Electric field of a laser pulse and corresponding vector potential. Bottom: Unsaturated ionization rate $w(t)$ and electron emission rate dZ/dt in the saturated case.

contrast, the electron emission rate would be proportional to the ionization rate $w(t)$. Thus, compared to the non-saturated case, the instant of maximum electron emission shifts to an earlier optical half-cycle of the field. In addition, the preferred emission time within the half-cycle moves away from the peak of the field toward earlier times. The latter effect is especially relevant since the vector potential $A(t)$ (represented as a colormap in the upper panel of Fig. 4) is zero around the peaks of the field. In the presence of saturation, most electrons are born in regions with nonzero vector potential and acquire a drift momentum, proportional to $A(t_i)$, which leads to higher current. Here, t_i is the birth time of an electron i , which can be extracted from Eq. (3).

To further investigate the signal scaling in saturated ionization, both the intensity scaling and the radial intensity distribution in the focus need to be considered. To model the detected signal, we examine the total drift momentum acquired by all free electrons in the volume under consideration. In the spirit of Ref. 35, the final velocity of an electron born at t_i , $v_i = -\frac{e}{m}A(t_i)$, can be written in terms of the vector potential $A(t_i) = -\int_{-\infty}^{t_i} E(t) dt$. To consider electrons moving in different directions, we take the vectorial sum over all velocities, $\bar{v} = \sum_i v_i$, which yields an estimate of the mean signal at a given CEP. In all cases, we assume that each newly freed electron starts with zero kinetic energy. For a few-cycle laser pulse, the net velocity \bar{v} is a function of CEP. For symmetry reasons, \bar{v} is expected to change sign upon a π -shift of the CEP. Accordingly, we define the magnitude \hat{S} of the CEP-dependent signal as the difference between the maximum and minimum values for \bar{v} as a function of CEP φ ,

$$\hat{S} = \frac{1}{N} \cdot \left(\max_{\varphi \in [0; 2\pi]} (\bar{v}(\varphi)) - \min_{\varphi \in [0; 2\pi]} (\bar{v}(\varphi)) \right), \quad (4)$$

where we normalize by the number of generated electrons N . The quantity \hat{S} is a measure of the contrast of the net average drift momentum per emitted charge carrier, and thus a measure of the phase sensitivity of the detected current. Normalization per particle allows for the interpretation of saturation phase effects: If the birth times of the electrons remained unchanged, meaning no temporal shift occurred due to saturation, the drift momentum per particle, and thus \hat{S} , would scale linearly with the field strength.

Calculating \hat{S} for different peak intensities, see Fig. 5(a), we indeed find that the phase signal per particle experiences a boost of nearly one order of magnitude at an intensity of around $5 \times 10^{14} \text{ W/cm}^2$.

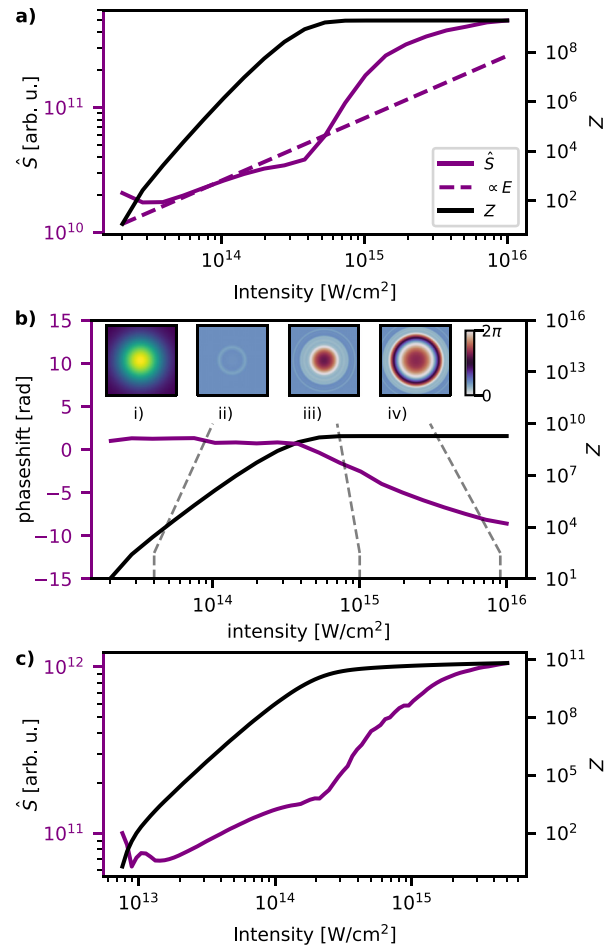


FIG. 5. (a) Ion yield Z and expected signal \hat{S} in the saturated case, neglecting spatial variations of the intensity. The dashed line indicates the $\propto \sqrt{I}$ scaling. (b) Phase shift between the final electron momentum and the driving pulse CEP. The inset (i) shows a Gaussian beam profile and insets (ii)–(iv) show the corresponding spatial phase distribution for different peak intensities. (c) Scaling of the expected signal \hat{S} with intensity including the spatially varying phase in (b).

In this calculation, we assumed a ground state population of 3×10^9 particles in a finite region with constant intensity. The number of particles is estimated assuming a particle density $n \approx 1 \times 10^{23} \text{ m}^{-3}$ and a typical focal volume. The intensity denotes the instantaneous peak intensity and directly entered the calculations. For intensities above $2 \times 10^{15} \text{ W/cm}^2$, the scaling of the signal contrast becomes flatter than $\propto E$. This flattening indicates that while the shift of the injection time within the half-cycle is the dominant mechanism for the signal boost, the jump to earlier half-cycles becomes the predominant effect at high intensities.

The maximum of $\bar{v}(\varphi)$ shifts with intensity. This phase shift is determined by fitting a sinusoidal function to the calculated curve $\bar{v}(\varphi)$. We find that it sets in at the saturation point, see Fig. 5(b). It is a direct consequence of the temporal shift of the electron injection time and becomes a function of position due to the focal intensity distribution. For illustration, we show the calculated spatial dependence of the phase shift in the insets of Figs. 5(b) (ii)–(iv) for a Gaussian beam

profile Fig. 5(b) i). Notably, there are different shells around the focus that lead to a different phase of the signal, describing that the net movement of electrons from different radii proceeds in different directions.

To estimate the effect of this phase shift, we include the radial intensity profile by computing \bar{v} for different intensities and scaling it by the number of particles in a thin cylindrical shell in the focal plane. The number of particles in a shell of length d , radius r , and thickness dr is given by $N_0(r) = nd\pi(2rdr + dr^2)$. We can then calculate \hat{S} after summing over all radii. The results are presented in Fig. 5(c). As shown, the signal still exhibits an enhancement at an intensity just above 2×10^{14} W/cm². However, the scaling is less pronounced as compared to the case where the spatial intensity profile was not considered. At intensities above 2×10^{15} W/cm², the signal scales linearly ($\propto E$) again.

The calculations predict a signal enhancement around the saturation intensity of the ionization process. The spatial intensity distribution in the focal volume, however, causes a spatially varying phase of the CEP dependence that tends to smear out the detected signal, especially at high intensities. Integration over the focal volume reveals that even though both effects counteract each other, the net signal boost occurs for intensities in the range of $(4-9) \times 10^{14}$ W/cm². This intensity range represents a “sweet spot” where the interplay of the different saturation effects enhances the overall signal, and aligns with the intensity of optimal device resolution observed experimentally.

The measured phase sensitivity decreases again for intensities above 8×10^{14} W/cm², which contrasts with the numerical model, where the signal increases according to the $\propto E$ -scaling. This discrepancy indicates that the model does not fully capture the experimental conditions: In this regime, the target is heavily ionized and the propagation of the free charges needs to be considered. In particular, significant electron-ion scattering and electron-ionic mean field interactions are expected.¹⁸ Since scattering introduces randomness to the movement of the electrons and, consequently, leads to a loss of the CEP information they carry, an overall decrease in CEP-dependent signal is expected for high intensities.

The phase shift between the CEP and the final electron momentum we identified in the calculations prevents a measurement of the absolute CEP without calibration. However, this is a common feature with other CEP sensing techniques.⁴⁻⁶ Additionally, the phase shift results in an intensity-phase-coupling equivalent to 20 mrad noise for 1% intensity fluctuations as extracted from Fig. 5(b). Due to phase differences between the CEP meter and the experiment, however, the absolute CEP is typically not of interest.

In conclusion, we have demonstrated that single-shot CEP detection in gas-gap devices is a robust measurement technique, even over extended periods of time. We investigated the performance of the device depending on the input intensity and we found an optimum intensity for which best performance is obtained in terms of sensitivity and precision. Our theoretical investigations have revealed that the saturation of ionization shifts the electron injection in time, which enhances the phase dependence of the signal. This enhancement is counteracted by the spatial dependence of the phase shift imprinted by the focal intensity distribution. The combination of both spatial and temporal effects results in a net signal enhancement within a well-defined intensity range. The latter is consistent with the optimum intensity region identified in our experiments, which provides an explanation for the enhanced device performance at this intensity.

We are grateful for the assistance of Harald Haas in designing the electronic circuitry. We thank Ferenc Krausz for providing suitable laboratory space. J.B. acknowledges support from the Max Planck School of Photonics.

This work was funded by the Max Planck School of Photonics (J.B.), the European Research Council via FETopen PetaCOM and FETLaunchpad FIELDTECH (B.B. and M.F.K.), and the U.S. Department of Energy, Office of Science, Basic Energy Sciences (No. DE-AC02-76SF00515), (M.F.K.).

AUTHOR DECLARATIONS

Conflict of Interest

The authors have no conflicts to disclose.

Author Contributions

Johannes Blöchl: Formal analysis (lead); Investigation (lead); Methodology (equal); Software (lead); Validation (lead); Visualization (lead); Writing – original draft (lead); Writing – review & editing (equal). **Maximilian F. Seeger:** Investigation (equal); Methodology (equal); Validation (equal); Writing – original draft (equal); Writing – review & editing (equal). **Hartmut Schröder:** Conceptualization (supporting); Methodology (equal); Supervision (supporting); Validation (equal); Writing – original draft (equal); Writing – review & editing (equal). **Minjie Zhan:** Investigation (supporting); Writing – original draft (supporting); Writing – review & editing (equal). **Alexander Guggenmos:** Funding acquisition (equal); Project administration (equal); Resources (equal); Validation (supporting); Writing – original draft (supporting); Writing – review & editing (equal). **Thomas Nubbemeyer:** Investigation (equal); Project administration (equal); Resources (equal); Supervision (supporting); Validation (supporting); Writing – original draft (equal); Writing – review & editing (equal). **Matthias F. Kling:** Conceptualization (equal); Funding acquisition (equal); Project administration (equal); Resources (lead); Supervision (supporting); Validation (equal); Writing – original draft (equal); Writing – review & editing (equal). **Boris Bergues:** Conceptualization (equal); Funding acquisition (equal); Methodology (equal); Project administration (equal); Supervision (equal); Validation (equal); Writing – original draft (equal); Writing – review & editing (equal).

DATA AVAILABILITY

The data that support the findings of this study are available from the corresponding author upon reasonable request.

REFERENCES

- ¹F. Krausz and M. Ivanov, *Rev. Mod. Phys.* **81**, 163 (2009).
- ²T. Rathje, N. G. Johnson, M. Möller, F. Süßmann, D. Adolph, M. Kübel, R. Kienberger, M. F. Kling, G. G. Paulus, and A. M. Saylor, *J. Phys. B: At. Mol. Opt. Phys.* **45**, 074003 (2012).
- ³F. Calegari, G. Sansone, S. Stagira, C. Vozzi, and M. Nisoli, *J. Phys. B: At. Mol. Opt. Phys.* **49**, 062001 (2016).
- ⁴T. Wittmann, B. Horvath, W. Helml, M. G. Schätzel, X. Gu, A. L. Cavalieri, G. G. Paulus, and R. Kienberger, *Nat. Phys.* **5**, 357 (2009).
- ⁵G. G. Paulus, F. Lindner, H. Walther, A. Baltuška, E. Goulielmakis, M. Lezius, and F. Krausz, *Phys. Rev. Lett.* **91**, 253004 (2003).
- ⁶M. Kakehata, H. Takada, Y. Kobayashi, K. Torizuka, Y. Fujihira, T. Homma, and H. Takahashi, *Opt. Lett.* **26**, 1436 (2001).

- ⁷X. Ren, A. M. Summers, K. R. P., A. Vajdi, V. Makhija, C. W. Fehrenbach, N. G. Kling, K. J. Betsch, Z. Wang, M. F. Kling, K. D. Carnes, I. Ben-Itzhak, C. Trallero-Herrero, and V. Kumarappan, *J. Opt.* **19**, 124017 (2017).
- ⁸M. Kurucz, S. Tóth, R. Flender, L. Haizer, B. Kiss, B. Persielle, and E. Cormier, *Opt. Express* **27**, 13387 (2019).
- ⁹C. Guo, M. Miranda, A.-K. Raab, A.-L. Viotti, P. T. Guerreiro, R. Romero, H. Crespo, A. L'Huillier, and C. L. Arnold, *Opt. Lett.* **48**, 5431 (2023).
- ¹⁰Y. Yang, M. Turchetti, P. Vasireddy, W. P. Putnam, O. Karnbach, A. Nardi, F. X. Kärtner, K. K. Berggren, and P. D. Keathley, *Nat. Commun.* **11**, 3407 (2020).
- ¹¹Y. Liu, J. E. Beetar, J. Nesper, S. Gholam-Mirzaei, and M. Chini, *Nat. Photonics* **16**, 109 (2022).
- ¹²V. Hanus, B. Fehér, V. Csajbók, P. Sándor, Z. Pápa, J. Budai, Z. Wang, P. Paul, A. Szeghalmi, and P. Dombi, *Nat. Commun.* **14**, 5068 (2023).
- ¹³F. Ritzkowski, M. Yeung, E. Bebeti, T. Gebert, T. Matsuyama, M. Budden, R. E. Mainz, H. Cankaya, K. K. Berggren, G. M. Rossi, P. D. Keathley, and F. X. Kärtner, *Nat. Commun.* **15**, 10179 (2024).
- ¹⁴A. Rossetti, M. Falk, A. Leitenstorfer, D. Brida, and M. Ludwig, *Nanophotonics* **13**, 2803 (2024).
- ¹⁵A. Schiffrin, T. Paasch-Colberg, N. Karpowicz, V. Apalkov, D. Gerster, S. Mühlbrandt, M. Korbman, J. Reichert, M. Schultze, S. Holzner, J. V. Barth, R. Kienberger, R. Ernstorfer, V. S. Yakovlev, M. I. Stockman, and F. Krausz, *Nature* **493**, 70 (2013).
- ¹⁶T. Paasch-Colberg, A. Schiffrin, N. Karpowicz, S. Kruchinin, Ö. Sağlam, S. Keiber, O. Razskazovskaya, S. Mühlbrandt, A. Alnaser, M. Kübel, V. Apalkov, D. Gerster, J. Reichert, T. Wittmann, J. V. Barth, M. I. Stockman, R. Ernstorfer, V. S. Yakovlev, R. Kienberger, and F. Krausz, *Nat. Photonics* **8**, 214 (2014).
- ¹⁷M. Kubullek, Z. Wang, K. von der Brelje, D. Zimin, P. Rosenberger, J. Schötz, M. Neuhaus, S. Sederberg, A. Staudte, N. Karpowicz, M. F. Kling, and B. Bergues, *Optica* **7**, 35 (2020).
- ¹⁸J. Schötz, A. Maliakkal, J. Blöchl, D. Zimin, Z. Wang, P. Rosenberger, M. Alharbi, A. M. Azzeer, M. Weidman, V. S. Yakovlev, B. Bergues, and M. F. Kling, *Nat. Commun.* **13**, 962 (2022).
- ¹⁹B. Kim, J. u Shin, W. Cho, Y. H. Kim, K. H. Yeom, and K. T. Kim, *Opt. Express* **32**, 33795 (2024).
- ²⁰B. Bergues, *Opt. Express* **20**, 25317 (2012).
- ²¹M. Kübel, K. J. Betsch, N. G. Johnson, U. Kleineberg, R. Moshhammer, J. Ullrich, G. G. Paulus, M. F. Kling, and B. Bergues, *New J. Phys.* **14**, 093027 (2012).
- ²²D. Hoff, F. J. Furch, T. Witting, K. Rühle, D. Adolph, A. M. Sayler, M. J. J. Vrakking, G. G. Paulus, and C. P. Schulz, *Opt. Lett.* **43**, 3850 (2018).
- ²³A. Korobenko, K. Johnston, M. Kubullek, L. Arissian, Z. Dube, T. Wang, M. Kübel, A. Y. Naumov, D. M. Villeneuve, M. F. Kling, P. B. Corkum, A. Staudte, and B. Bergues, *Optica* **7**, 1372 (2020).
- ²⁴T. Rybka, M. Ludwig, M. F. Schmalz, V. Knittel, D. Brida, and A. Leitenstorfer, *Nat. Photonics* **10**, 667 (2016).
- ²⁵M. Ludwig, A. K. Kazansky, G. Aguirregabiria, D. C. Marinica, M. Falk, A. Leitenstorfer, D. Brida, J. Aizpurua, and A. G. Borisov, *Phys. Rev. B* **101**, 241412 (2020a).
- ²⁶M. Ludwig, G. Aguirregabiria, F. Ritzkowski, T. Rybka, D. C. Marinica, J. Aizpurua, A. G. Borisov, A. Leitenstorfer, and D. Brida, *Nat. Phys.* **16**, 341 (2020b).
- ²⁷M. Miranda, C. L. Arnold, T. Fordell, F. Silva, B. Alonso, R. Weigand, A. L'Huillier, and H. Crespo, *Opt. Express* **20**, 18732 (2012).
- ²⁸C. J. G. J. Uiterwaal, C. R. Gebhardt, H. Schröder, and K.-L. Kompa, *Eur. Phys. J. D* **30**, 379 (2004).
- ²⁹L. V. Keldysh, *Sov. Phys. JETP* **20**, 1307 (1965).
- ³⁰M. V. Ammosov, N. B. Delone, and V. P. Krainov, *Sov. Phys. JETP* **64**, 1191 (1986).
- ³¹X. M. Tong, Z. X. Zhao, and C. D. Lin, *Phys. Rev. A* **66**, 033402 (2002).
- ³²A. Perelomov, V. Popov, and T. MV, *Sov. Phys. JETP* **23**, 924 (1966).
- ³³A. Velasco and C. Lavín, *J. Quant. Spectrosc. Radiat. Transfer* **169**, 122 (2016).
- ³⁴J. L. Holmes, M. Fingas, and F. Lossing, *Can. J. Chem.* **59**, 80 (1981).
- ³⁵P. B. Corkum, *Phys. Rev. Lett.* **71**, 1994 (1993).